Soft Matter

PAPER

View Article Online
View Journal | View Issue

Cite this: *Soft Matter*, 2023, **19**, 4706

Construction of micelles and hollow spheres *via* the self-assembly behavior of poly(styrene-*alt*-*p*HPMI) copolymers with poly(4-vinylpyridine) derivatives mediated by hydrogen bonding interactions†

Tzu-Ling Ma,[a] Wei-Ting Du[a] and Shiao-Wei Kuo *[ab]

Received 6th May 2023,
Accepted 31st May 2023

DOI: 10.1039/d3sm00595j

rsc.li/soft-matter-journal

This study describes the preparation of hydrogen bonding connected micelles, consisting of a poly(styrene-*alt*-(*para*-hydroxyphenylmaleimide)) [poly(S-*alt*-pHPMI)] core and a poly(4-vinylpyridine) (P4VP) derivative shell in a selective solvent. The aim was to modify hydrogen bonding interaction sites at the core/shell interface by synthesizing P4VP derivatives in three different sequences, namely, P4VP homopolymers, PS-*co*-P4VP random copolymers, and block copolymers. TEM images showed the successful self-assembly of poly(S-*alt*-pHPMI)/PS-*co*-P4VP inter-polymer complexes into spherical structures. To dissolve the core structures, 1,4-dibromobutane was used as a cross-linking agent to tighten the PS-*co*-P4VP shell. The morphologies, particle sizes, hydrogen bonding, cross-linking reaction, and core dissolution were confirmed by TEM, DLS, FTIR, and AFM analyses. Poly(S-*alt*-*p*HPMI)/PS_{41}-*r*-$P4VP_{59}$ hydrogen bonding connected micelles, cross-linked micelles, and hollow spheres were larger and more irregular than poly(S-*alt*-*p*HPMI)/P4VP inter-polymer complexes due to the random copolymer architecture and the decrease in intermolecular hydrogen bonds. However, poly(S-*alt*-*p*HPMI)/PS_{68}-*b*-$P4VP_{32}$ resulted in rod- or worm-like structures after core dissolution.

Introduction

Polymeric micelles have been extensively studied due to their potential in various applications such as drug delivery, sensing, and serving as charge carriers. As a result, researchers have investigated and developed various types of polymeric micelles to further enhance their potential uses.[1–6] The common strategy is using block copolymers, which act as amphiphilic surfactants that can self-assemble in a selective solvent to form micelle structures containing an insoluble core and a soluble shell. For example, a PS-*b*-P4VP self-assembly forms lamellae, double gyroids, and cylinders in bulk-state or spherical micelles in DMF with a PS core and a P4VP corona.[7–11] However, this strategy to form desirable micelle structures is restricted by the molecular weight of block copolymers, leading to a complicated synthesis process.[12–14] Furthermore, the covalent bond interaction at the core and shell interface made the core structure hard to remove to obtain further hollow spheres, for instance, *via* chemical degradation or calcination.[15,16]

To overcome these limitations, an alternative method has been developed to create desirable micelle structures in a more convenient way. Noncovalently connected micelles (NCCMs) are formed by a strategy of inter-polymer complexation, which involves a specific interacting driving force to form micelles, especially hydrogen bonding to physically interact at the core/shell interface. Committed to obtain more regular aggregates, the content of hydrogen bonded donors and the interaction sites at the core/shell interface should be designed. Guo and Jiang proposed a block-copolymer-free strategy, using solvent/precipitant mixtures to form self-assembly micelle structures.[17] The general principle is utilizing polymer A and B with homogenous or randomly repeating units, which contain hydrogen bonded donor/acceptor pairs to form a complementary interaction with each other. Selected solvents are C and D; C is good for polymer A but a non-solvent for polymer B, and D is good for both polymers A and B. When a B/D solution is dropped into a A/C solution, B chains aggregate, and then they are surrounded by A chains due to the A/B hydrogen bonding interaction. Hence, micelle-like structures are formed with an insoluble B

[a] *Department of Materials and Optoelectronic Science, Center of Crystal Research, National Sun Yat-Sen University, Kaohsiung 804, Taiwan. E-mail: kuosw@faculty.nsysu.edu.tw*
[b] *Department of Medicinal and Applied Chemistry, Kaohsiung Medical University, Kaohsiung 807, Taiwan*

† Electronic supplementary information (ESI) available. See DOI: https://doi.org/10.1039/d3sm00595j

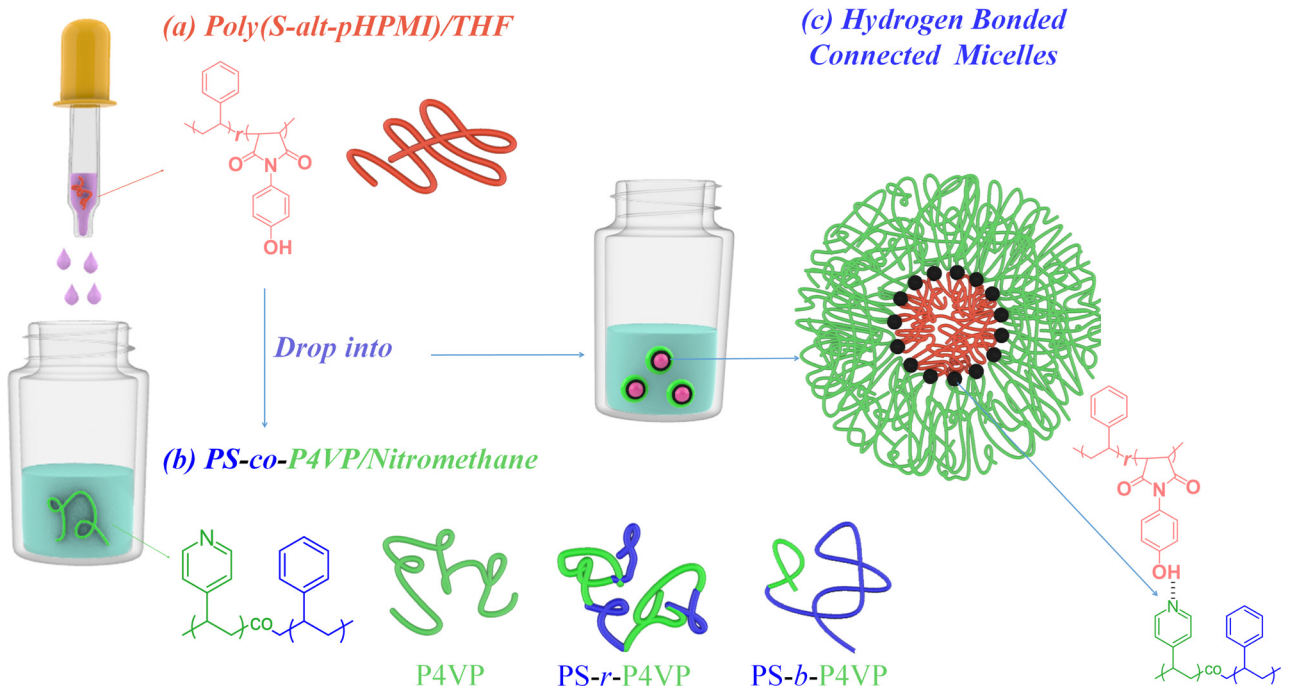

Scheme 1 Formation of hydrogen bonded connected micelles from poly(S-*alt*-*p*HPMI)/P4VP derivative complex (c) from (a) poly(S-*alt*-*p*HPMI) in a THF solution and dropped into (b) a PS-*co*-P4VP copolymer in nitromethane *via* intermolecular interaction between OH units of poly(S-*alt*-*p*HPMI) copolymers and pyridine units of P4VP derivatives.

core and a soluble A shell (Scheme 1). For example, Jiang *et al.* reported that a PS(OH)/chloroform solution was dropped into a P4VP/nitromethane solution, and PS(OH) and P4VP form self-assembly micelle structures containing a hydrogen bonding interface with the insoluble PS(OH) core and soluble P4VP shell. Furthermore, as the hydrogen bonded donors increase, the shape of particles change from spherical micelles to rod-like cluster networks, as the hydrogen bonding interaction sites at the core/shell interface increase.[18]

For the purpose of pursuing regular micelle structures, we chose poly(S-*alt*-*p*HPMI) as the polymeric micelle core, as the styrene repeating units in the alternating sequence could dilute hydrogen bonding donors effectively.[19] Besides, our previous report has showed that the intermolecular hydrogen bonding interactions of poly(S-*alt*-*p*HPMI)/P4VP binary blends were weak compared to poly(S-*alt*-*p*HPMI)/PVP binary blends.[19–21] Thus, we also selected homopolymer P4VP as a polymeric micelle corona, except to obtain sphere-like micelle structures. Subsequently, we synthesized a random copolymer, PS_{41}-*r*-$P4VP_{59}$, *via* free radical polymerization and a block copolymer, PS_{68}-*b*-$P4VP_{32}$, *via* anionic living polymerization.[22] Our aim was to reduce the hydrogen bonded acceptor gradually by designing different sequences of polymeric micelle shells, which interact with poly(S-*alt*-*p*HPMI) to adjust the hydrogen bonding interaction sites at the core/shell interface. Furthermore, we utilized 1,4-dibromobutane as a crosslinking agent to stabilize hollow spheres created by eliminating the core by a simple solvent dissolution method.[18] We confirmed the chemical structures of all PS-*co*-P4VP random copolymers by ^{1}H NMR spectroscopy and thermal analysis using DSC and TGA. The morphologies of micelles, micelles with cross-linked shells, and hollow spheres were examined by transmission electron microscopy (TEM). We also used FTIR spectroscopy to identify the difference in micelles, micelles with cross-linked shells, and hollow spheres and then discussed their hydrogen bonding interactions.

Experimental section

Materials

Styrene (99%), nitromethane (98%), and 1,4-dibromobutane (98%) were purchased from Alfa Aesar. 4-Vinylpyridine (95%), tetrahydrofuran (THF), methanol (MeOH), diethyl ether (Et_2O), and hexane were obtained from Acros Organics. Azobisisobutyronitrile (AIBN) was recrystallized from MeOH and purchased from SHOWA. *N*,*N*-Dimethylformamide (DMF) was acquired from J. T. Baker. Prior to the polymerization, the monomers and solvents were dried with CaH_2 overnight and distilled under vacuum. In addition, a poly(S-*alt*-*p*HPMI) alternating copolymer,[19] a P4VP homopolymer,[20] and a PS_{68}-*b*-$P4VP_{32}$ diblock copolymer[22] have been synthesized previously in our previous works.

Synthesis of PS_{41}-*r*-$P4VP_{59}$ random copolymers

To synthesize the PS_{41}-*r*-$P4VP_{59}$ random copolymer, a free radical copolymerization method was used. First, recrystallized AIBN (5 wt%) was placed in a 100 mL two-necked round-bottom flask, followed by the addition of dry THF (30 mL) to dissolve

the solid. Once the solution became clear, styrene (0.63 g, 6.02 mmol) and 4-vinylpyridine (0.63 g, 6.00 mmol) were added separately to the flask. The mixture was then reacted under N_2 at 70 °C and stirred for 24 hours.

The reaction was terminated by exposing the solution to air for 1 hour, and then the solution was concentrated under reduced pressure until turbid. The final copolymers were dropped into cold Et_2O, and the resulting precipitates were purified twice with THF/cold Et_2O. The white solid obtained was then dried under vacuum for 5 days. Yield: 0.221 g; FTIR (KBr, cm^{-1}): 3024 (aromatic C–H stretching), 2928 (alkanes C–H stretching), 1598 (rings of styrene and pyridine), 993 (pyridine rings C–H bending); ^{1}H NMR (500 MHz, chloroform-d, δ, ppm): 1.28–2.07 (3H, CH_2CH), 6.12–7.23 (7H, C═CH in styrene and pyridine rings), 8.04–8.55 (2H, N═CH in pyridine); thermal decomposition temperatures (T_{d5} and T_{d10}) were 313 and 346 °C; number-average molecular weight M_n: 30 400 g mol^{-1}, polydispersity index (PDI): 1.201.

Preparation of hydrogen bonding connected micelles

For the preparation of the micelle solution, P4VP, PS_{41}-*r*-$P4VP_{59}$, and PS_{68}-*b*-$P4VP_{32}$ (1.82 mg each) were dissolved in nitromethane (9 mL) in three separate vial bottles (Scheme 1(b)). Next, 1 mL of a poly(S-*alt*-*p*HPMI)/THF solution (4 mg mL^{-1}) (Scheme 1(a)) was slowly added to each vial over a period of approximately 5 minutes. The addition of the poly(S-*alt*-*p*HPMI)/THF solution caused the appearance of the solution to change from colorless to canary yellow, indicating the formation of micelles (Scheme 1(c)). The resulting mixture was stirred at ambient temperature overnight and kept for 3 days before use for further measurements.

Micelles of cross-linked shell

To crosslink the hydrogen bonding connected micelles (Scheme 2(a)), 1,4-dibromobutane was added to each of the three micelle solutions. The molar ratio of bromide units in 1,4-dibromobutane to pyridine units in the copolymer was 2 : 1.

The resulting mixture was slightly stirred at 60 °C for two days to facilitate the crosslinking process, as shown in Scheme 2(b).

Formation of hollow spheres

After the crosslinking process, the micelle solution with a cross-linked shell was mixed with an equal volume of DMF. The resulting mixture was slightly stirred at ambient temperature for 20 hours and then kept for 5 days to ensure that the core of the micelles was thoroughly washed with DMF, as shown in Scheme 2(c).

Results and discussion

Characterizations of PS-*co*-P4VP copolymers

In this study, we aimed to investigate how the composition and sequence distribution of P4VP affect the self-assembled structures when interacting with a poly(S-*alt*-*p*HPMI) alternating copolymer *via* hydrogen bonding. To do so, we synthesized two copolymers: a PS_{41}-*r*-$P4VP_{59}$ random copolymer and a PS_{68}-*b*-$P4VP_{32}$ diblock copolymer *via* free radical polymerization

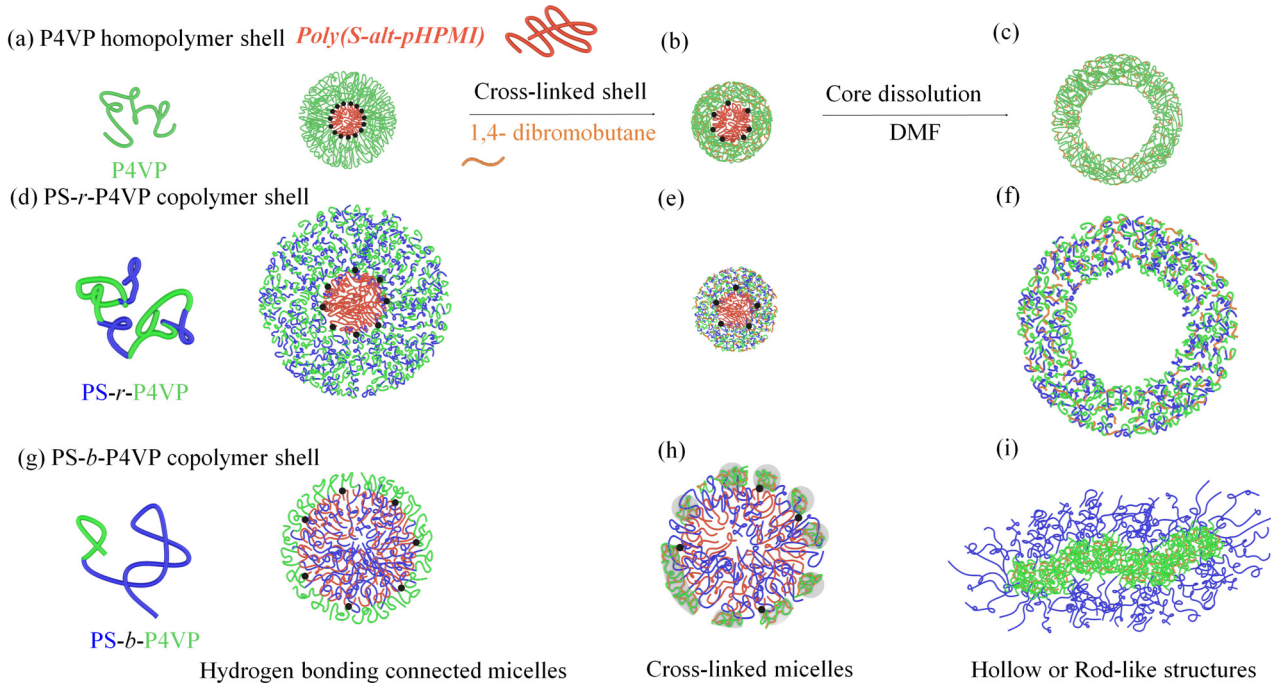

Scheme 2 (a, d and g) Hydrogen bonding connected micelles, (b, e and h) crosslinked micelles with 1,4-dibromobutane, and (c, f and i) hollow sphere- or rod-like structure after dissolution in the DMF solution from poly(S-*alt*-*p*HPMI) with (a–c) P4VP homopolymers, (d–f) PS_{41}-*r*-$P4VP_{59}$ copolymers, and (g–i) PS_{68}-*b*-$P4VP_{32}$ copolymer complexes, respectively.

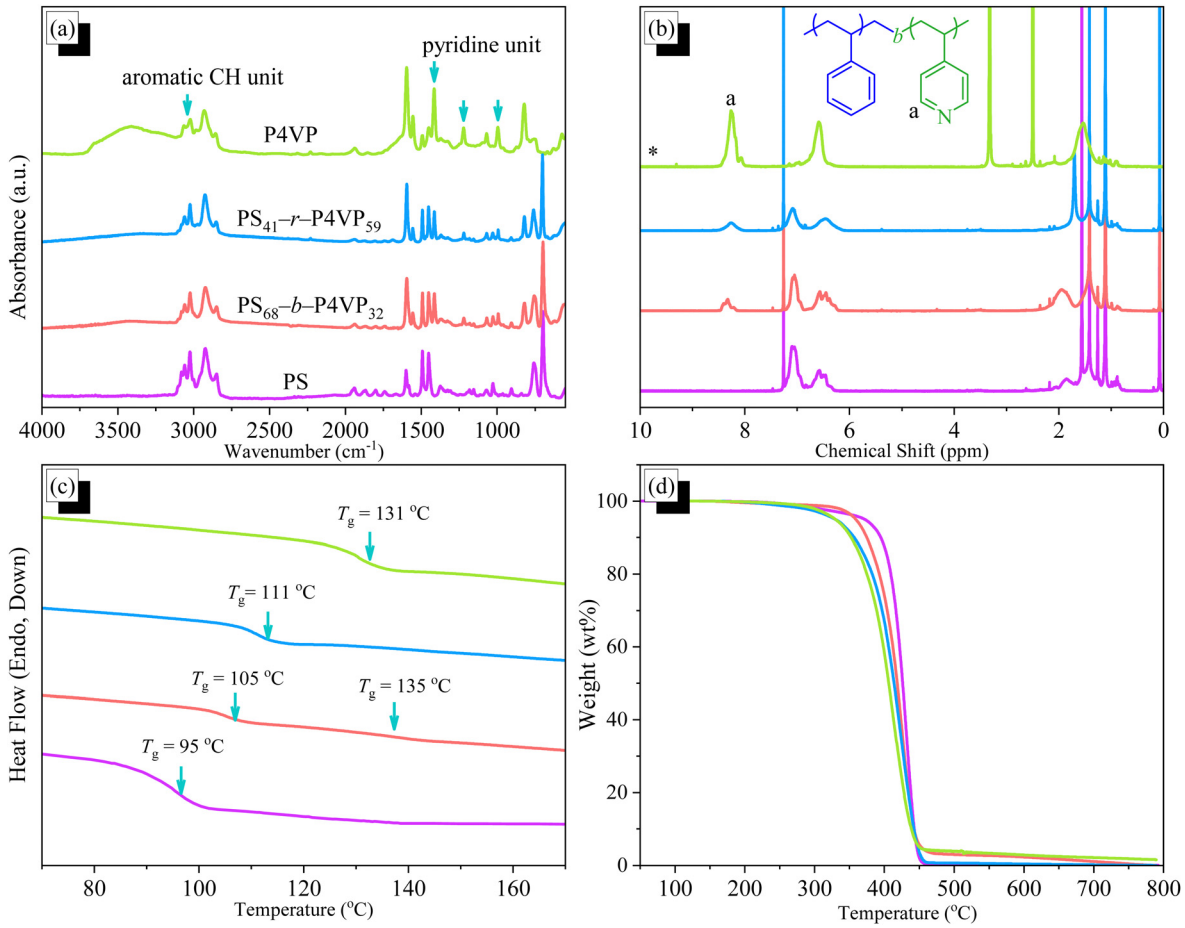

Fig. 1 (a) FTIR spectra, (b) 1H NMR spectra (chloroform-*d*), * (DMSO-d_6), (c) DSC, and (d) TGA thermal analyses of pure PS homopolymers, PS_{68}-*b*-$P4VP_{32}$ copolymers, and PS_{41}-*r*-$P4VP_{59}$ copolymers and pure P4VP homopolymers.

and anionic living polymerization, respectively. The compositions and chemical structures of these two copolymers were confirmed by FTIR and NMR analyses. The FTIR spectra (Fig. 1(a)) showed that despite having different sequence distributions, both copolymers had similar profiles because the vibrations of the aromatic rings, pyridine rings, and polymer backbone were identical. However, to distinguish the composition differences of these copolymers, we identified some specific peaks. For instance, we observed that the pyridine units in both PS-*co*-P4VP copolymers exhibited C-N stretching vibrations at 1416 cm^{-1} and 1222 cm^{-1}, which were absent in pure PS.[23,24] Additionally, the absorption bands at 993 cm^{-1} were due to C–H bending in pyridine rings, and this information was critical to discuss the hydrogen bond interactions.[25–27]

In addition, the ^{1}H NMR spectra (Fig. 1(b)) showed signals at 6.08–6.77 and 6.78–7.22 ppm, which represented protons in the aromatic and pyridine rings, respectively. Moreover, the signals at 8.03–8.49 ppm (peak a) corresponded to two protons in pyridine rings that were located nearby the nitrogen atoms.[28,29] By integrating these three peaks, we confirmed the repeat unit ratio of the copolymers. The styrene/4-vinylpyridine ratio of PS_{41}-*r*-$P4VP_{59}$ was approximately 41.4 : 58.6, while that of PS_{68}-*b*-$P4VP_{32}$ was 67.9 : 32.1, which were the ratios used in this study. The thermal properties of pure PS, pure P4VP, and the two PS-*co*-P4VP copolymers were analyzed by DSC, as shown in Fig. 1(c). The glass transition temperatures (T_g) of pure PS and P4VP were found to be 95 °C and 131 °C, respectively, which were consistent with previous studies.[30,31] Notably, the PS_{68}-*b*-$P4VP_{32}$ diblock copolymer exhibited two T_{gs} at around 105 and 135 °C, which were similar to those of the PS and P4VP segments, respectively. This result was attributed to the microphase separation in the diblock copolymer.[32] In contrast, the PS_{41}-*r*-$P4VP_{59}$ random copolymer displayed only one T_g, indicating that the random sequence distribution provided better miscibility.[33] Additionally, the TGA results of the two homopolymers and copolymers are presented in Fig. 1(d). The data suggested that pure PS had better thermal stability than P4VP, which is consistent with previous studies. The two copolymers were found to be located between the two homopolymers, as expected, indicating that their thermal stability was intermediate.

Preparation and morphology of poly(S-*alt*-*p*HPMI)/PS-*co*-P4VP hydrogen bonding connected micelles

In this study, we selected poly(S-*alt*-*p*HPMI) alternating copolymers and PS-*co*-P4VP copolymers with random and block sequences as

complementary polymer pairs to form micelles because of their hydrogen bonding interaction. However, the precipitate of inter-polymer complexation in the solution is usually irregular unless a selective solvent is used to form micelles that contained a hydrogen bonding interface in the middle of the core/shell. We found that THF was a suitable solvent for both types of polymers, while nitromethane was only suitable for PS-*co*-P4VP copolymers.

To prepare hydrogen bonding connected micelles, a selective solvent consisting of THF/nitromethane (v/v, 1/9) was used. The resulting micelles contained a poly(S-*alt*-*p*HPMI) core and a PS-*co*-P4VP shell. When the solution of poly(S-*alt*-*p*HPMI)/THF was added to PS-*co*-P4VP/nitromethane, the mixture changed from colorless to canary yellow, as shown in the inset picture in Fig. 2(a). This change in color indicated that the core of poly(S-*alt*-*p*HPMI) was successfully stabilized by PS-*co*-P4VP connected to a hydrogen bonding interface due to hydroxyl groups and pyridine rings, as shown in Scheme 1(c).

Poly(S-*alt*-*p*HPMI)/P4VP hydrogen bonding connected micelles

Fig. 2 presents TEM images and DLS analysis results of the poly(S-*alt*-*p*HPMI)/P4VP hydrogen bonding connected micelles. The TEM images showed that the morphologies of poly(S-*alt*-*p*HPMI)/P4VP micelles were spherical, with a diameter of approximately 100 nm, as shown in Fig. 2(a) and 2(b). However, the density of the pure P4VP shell was too low to observe the core/shell structure clearly, as shown in Scheme 2(a). In order

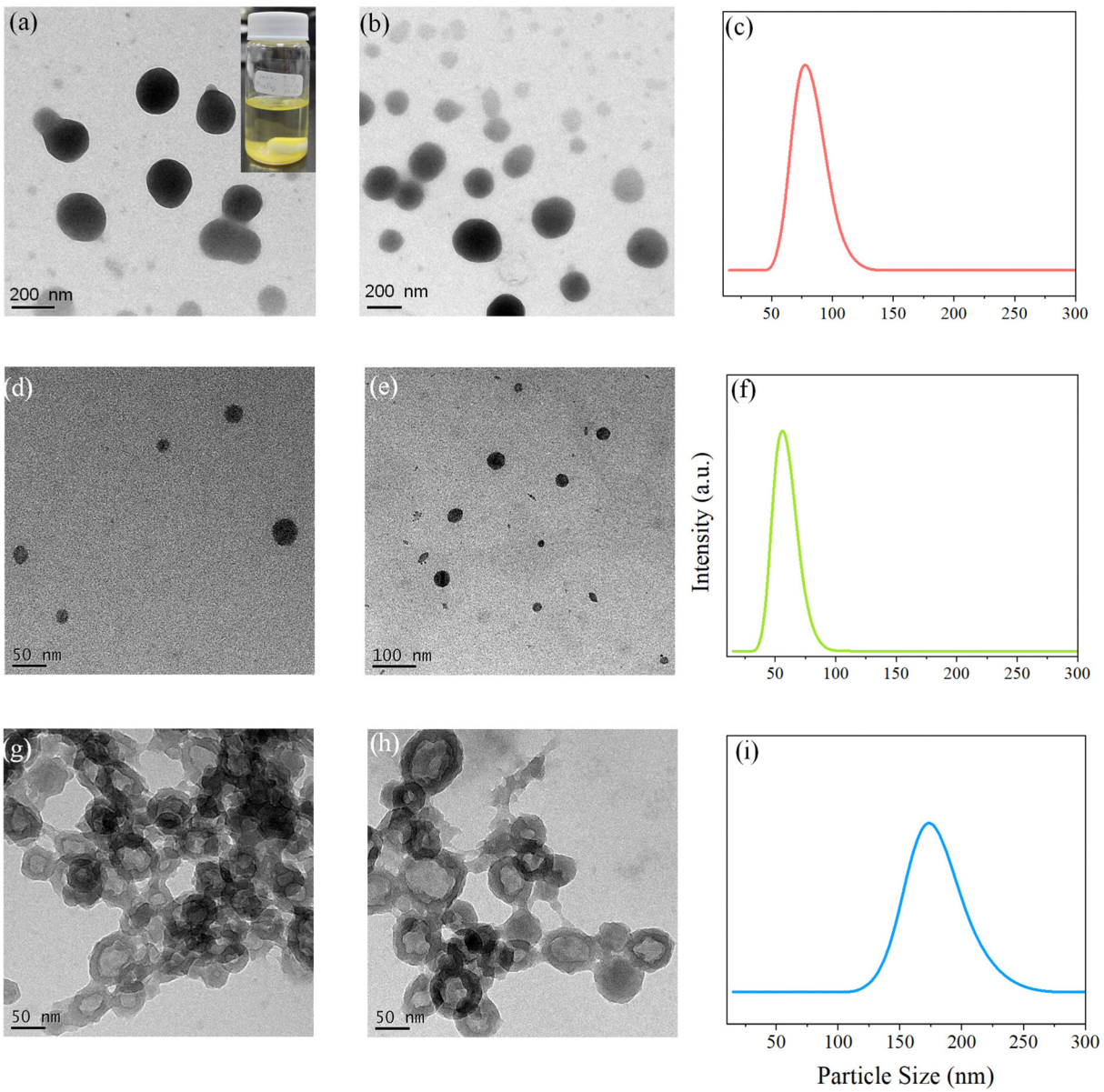

Fig. 2 (a and b) TEM images and (c) DLS analysis results of hydrogen bonding connected micelles, (d and e) TEM images and (f) DLS analysis results of the cross-linked micelles with 1,4-dibromobutane, and (g and h) TEM images and (i) DLS analysis of the hollow spheres after dissolution in the DMF solution from the poly(S-*alt*-*p*HPMI)/P4VP inter-polymer complex (all TEM images show staining with I_2).

to obtain hollow spheres, we used 1,4-dibromobutane as a cross-linker to tighten the shell structure. The TEM images in Fig. 2(d)–(e) show that the morphologies of poly(S-*alt*-*p*HPMI)/P4VP micelles with cross-linked shells still maintained a spherical shape, but the size of the spheres was smaller than that of the hydrogen bonding connected micelles, as shown in Scheme 2(b). Additionally, DLS measurements showed that the particle size of the poly(S-*alt*-*p*HPMI)/P4VP micelles changed from approximately 77 nm to 52 nm after the shell was cross-linked with 1,4-dibromobutane, as shown in Fig. 2(c) and 2(f). This result indicates that the P4VP shell was successfully tightened by the cross-linker. Finally, we used DMF to wash the poly(S-*alt*-*p*HPMI) core, and the TEM images in Fig. 2(g) and (h) showed a clear contrast between the shell and the center of the spheres. Furthermore, DLS measurements showed that the particle size of the resulting hollow spheres increased significantly to approximately 175 nm, as shown in Fig. 2(i). This result suggests that DMF acted as a dilute solution, causing the shell to swell, as shown in Scheme 2(c).[18] Similar profiles and particle sizes of the poly(S-*alt*-*p*HPMI)/P4VP micelles, micelles with cross-linked shells, and hollow spheres were also obtained by AFM, as shown in Fig. S1 (ESI†).

The FTIR spectra in Fig. 3 were used to confirm whether the P4VP shell had successfully formed hydrogen bonds with the poly(S-*alt*-*p*HPMI) core, whether the shell was cross-linked with 1,4-dibromobutane, and whether the poly(S-*alt*-*p*HPMI) alternating copolymer was removed by DMF washing. First, the FTIR absorption spectrum of the poly(S-*alt*-*p*HPMI)/P4VP hydrogen bonding connected micelles in Fig. 3(a) showed a band at 993 cm^{-1}, which is characteristic of the free pyridine units in pure P4VP. After the addition of poly(S-*alt*-*p*HPMI) alternating copolymers, we observed the hydrogen-bonded pyridine ring at 1005 cm^{-1}, which has been widely discussed in previous studies.[19,20] This result indicates that hydrogen bonding occurred between the P4VP shell and the poly(S-*alt*-*p*HPMI) core, as expected. Second, the intensity of absorption peaks at 2926 cm^{-1} (C–H stretching) increased, indicating that the P4VP shell was crosslinked with 1,4-dibromobutane to produce the [–(Py)CH–CH_2–CH(Py)–] backbone,[34–36] while the intensity of absorption peaks at 1005 cm^{-1} decreased, indicating that the hydrogen-bonded pyridine rings on the P4VP shell were replaced with crosslinked pyridine rings (Fig. 3(b)). Finally, after adding DMF, the peaks at 1712 cm^{-1} (symmetric C═O stretching of maleimide units in poly(S-*alt*-*p*HPMI)) disappeared (Fig. 3(c)).[19,20] A new peak at 1665 cm^{-1} (C═N^+ stretching) appeared, suggesting that the poly(S-*alt*-*p*HPMI) core was thoroughly washed with DMF to form hollow spheres.[37] The reason for the poly(S-*alt*-*p*HPMI) core being thoroughly washed out by DMF is the stronger intermolecular hydrogen bonding interaction between the hydroxyl groups in DMF and the maleimide units in poly(S-*alt*-*p*HPMI) compared to the hydrogen bonding interaction between the hydroxyl groups and pyridine units. This phenomenon has been extensively discussed in previous studies.[38]

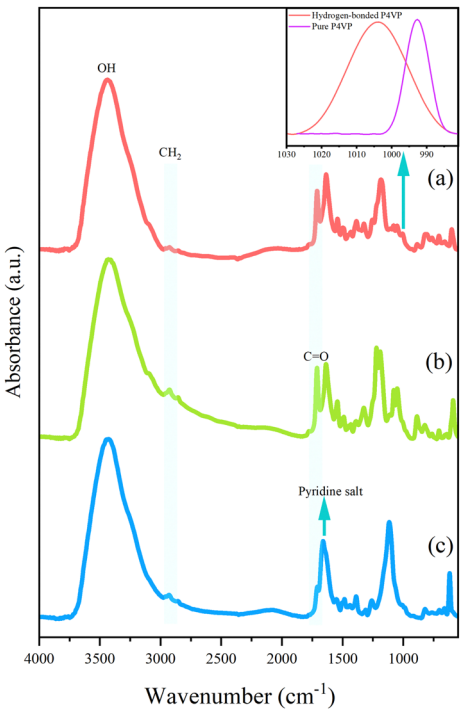

Fig. 3 FTIR spectra of (a) hydrogen bonding connected micelles, (b) cross-linked micelles with 1,4-dibromobutane, and (c) the hollow spheres after dissolution in the DMF solution from the poly(S-*alt*-*p*HPMI)/P4VP inter-polymer complex.

Poly(S-*alt*-*p*HPMI)/PS_{41}-*r*-$P4VP_{59}$ hydrogen bonding connected micelles

To investigate how the composition of P4VP affects the self-assembled structures when interacting with the poly(S-*alt*-*p*HPMI) alternating copolymer *via* hydrogen bonding, we prepared poly(S-*alt*-*p*HPMI)/PS_{41}-*r*-$P4VP_{59}$ hydrogen bonding connected micelles and analyzed them by TEM and DLS. The TEM images showed that the morphologies of these micelles were not as spherical as the poly(S-*alt*-*p*HPMI)/P4VP micelles (Fig. 4(a) and (b)). This suggests that the amount of intermolecular hydrogen bonding in this case is not enough to form regular spherical structures, as shown in Scheme 2(d). Subsequently, we also selected 1,4-dibromobutane to crosslink the shell structure. As shown in TEM results in Fig. 4(d) and (e), the morphologies of poly(S-*alt*-*p*HPMI)/PS_{41}-*r*-$P4VP_{59}$ micelles of cross-linked shell still remained similar, as shown in Scheme 2(e). However, it should be noted that the size of the micelles with cross-linked shells was smaller than that of the original size of the micelles without cross-linking, indicating that 1,4-dibromobutane cross-links the shell structure. This is likely due to the formation of multiple cross-links between neighboring P4VP chains, leading to the formation of smaller structures, which is consistent with the DLS measurement showing that the particle size changes from 290 nm to 80 nm (Fig. 4(c) and (f)), which revealed that the PS_{41}-*r*-$P4VP_{59}$ shell was also successfully fixed by 1,4-dibromobutane. Compared to Fig. 2(c) and 2(f), the particle size of poly(S-*alt*-*p*HPMI)/PS_{41}-*r*-$P4VP_{59}$ hydrogen bonding connected micelles was larger than that of poly(S-*alt*-*p*HPMI)/P4VP micelles and poly(S-*alt*-*p*HPMI)/P4VP micelles with cross-linked shells.

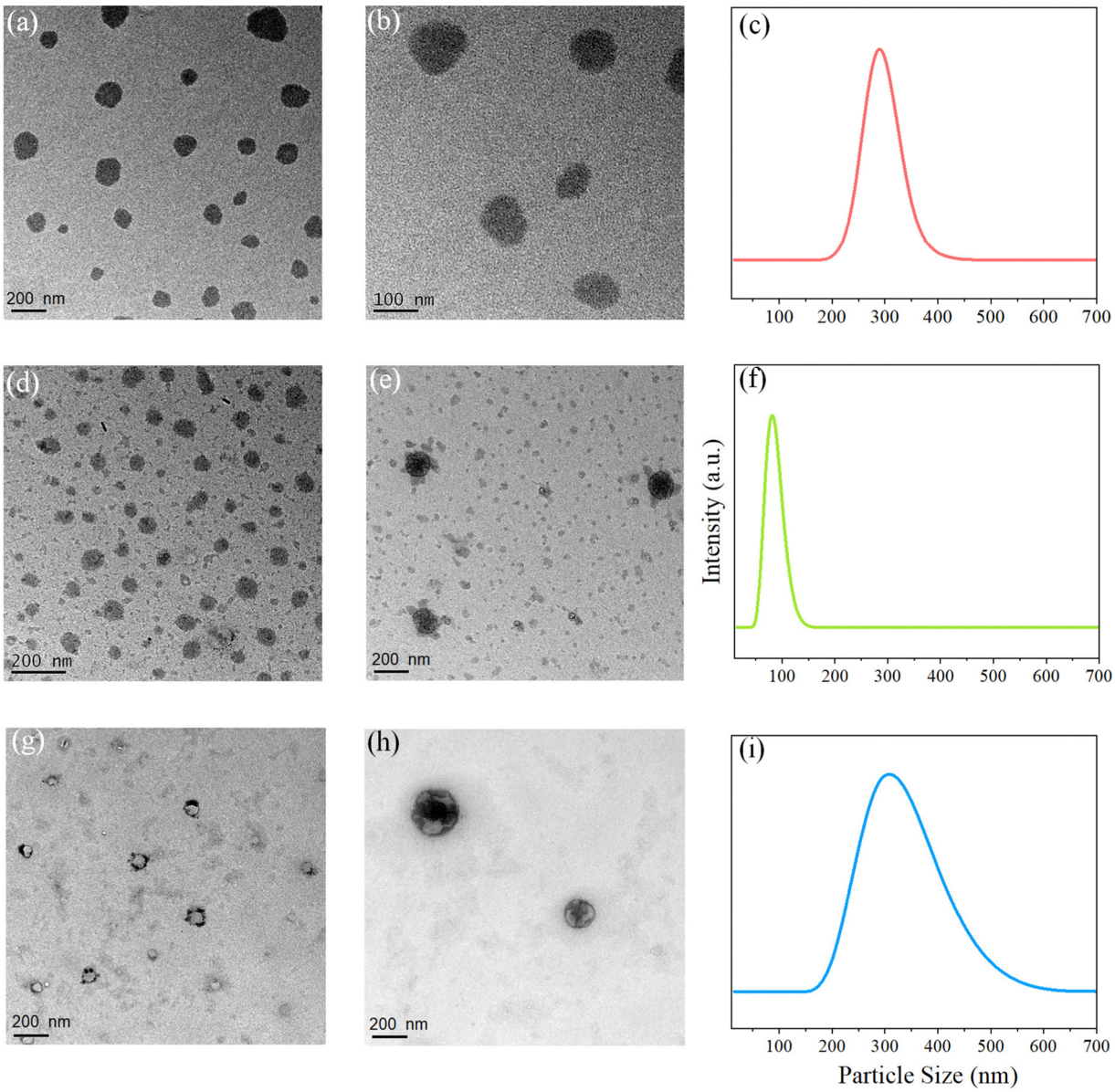

Fig. 4 (a and b) TEM images and (c) DLS analysis of hydrogen bonding connected micelles, (d and e) TEM images and (f) DLS analysis of the cross-linked micelles with 1,4-dibromobutane, and (g and h) TEM images and (i) DLS analysis of the hollow spheres after dissolution in DMF solution from poly(S-*alt*-*p*HPMI)/PS_{41}-*r*-$P4VP_{59}$ inter-polymer complex (all TEM images show staining with I_2).

This can be attributed to the fact that styrene units in the P4VP shell of PS_{41}-*r*-$P4VP_{59}$ were present in a lower concentration than that in pure P4VP, resulting in a decrease in the number of hydrogen bonding interaction sites at the core/shell interface that connect with hydroxyl units in poly(S-*alt*-*p*HPMI). This decrease in hydrogen bonding interactions led to chain aggregation of the inter-polymer complexation, resulting in an increase in free volume.[39] Furthermore, the random sequence distribution of PS_{41}-*r*-$P4VP_{59}$ also resulted in the interaction sites being less uniform than that of pure P4VP. In addition, DMF was again used to dissolve the poly(S-*alt*-*p*HPMI) core. Fig. 4(g) and (h) show that the hollow spheres were also successfully produced. Additionally, DLS measurements indicated that the particle size of the hollow spheres significantly increased to 315 nm (Fig. 4(i)), which once again suggested that DMF acted as a dilute solution and caused swelling of the shell, as shown in Scheme 2(f). AFM also showed similar morphologies and particle sizes for poly(S-*alt*-*p*HPMI)/PS_{41}-*r*-$P4VP_{59}$ hydrogen bonding connected micelles, micelles of cross-linked shells, and hollow spheres (Fig. S2, ESI†). Additionally, Fig. S3 (ESI†) displays the FTIR spectra of poly(S-*alt*-*p*HPMI)/PS_{41}-*r*-$P4VP_{59}$ hydrogen bonding connected micelles, micelles of cross-linked shells, and hollow spheres, which were similar to the results of the poly(S-*alt*-*p*HPMI)/P4VP hydrogen bonding connected micelle system. Therefore, we did not discuss the FTIR analyses of this system in detail.

Poly(S-*alt*-*p*HPMI)/PS_{68}-*b*-$P4VP_{32}$ Micelles

Since pure PS_{68}-*b*-$P4VP_{32}$ diblock polymers could self-assemble micelles in solutions, we were also interested in investigating the formation of micelles of poly(S-*alt*-*p*HPMI)/PS_{68}-*b*-$P4VP_{32}$ inter-polymer complexation mediated by hydrogen bonding interaction. Fig. 5 shows the TEM images and DLS data for poly(S-*alt*-*p*HPMI)/PS_{68}-*b*-$P4VP_{32}$ micelles, and we can observe that the morphologies of poly(S-*alt*-*p*HPMI)/PS_{68}-*b*-$P4VP_{32}$ inter-polymer complexation are still spherical. Additionally, the particle size appeared to be more polydisperse and smaller than that of poly(S-*alt*-*p*HPMI)/PS_{41}-*r*-$P4VP_{59}$ micelles, as shown in Fig. 5(a) and (b). Staining with I_2 and RuO_4 of poly(S-*alt*-*p*HPMI)/PS_{68}-*b*-$P4VP_{32}$ cross-linked micelles also displayed a similar spherical micelle structure. Since the PS block segment is insoluble in a nitromethane solution, it is assumed to be located in the inner micelle structure. In addition, Fig. S4 (ESI†) shows the DSC analysis results of poly(S-*alt*-*p*HPMI)/PS = 50/50 blend, indicating that two T_g behaviors were observed; however, the T_g behavior of the PS domain shifted from 95 °C to 140 °C and the poly(S-*alt*-*p*HPMI) domain from 259 °C shifted to 212 °C, indicating the partial miscibility of this mixture. However, the P4VP block segment of the shell can dissolve in a nitromethane solution and can also form hydrogen bonding interactions with a poly(S-*alt*-*p*HPMI) copolymer, as illustrated in Scheme 2(g). After applying the 1,4-dibromobutane crosslinking method to the poly(S-*alt*-*p*HPMI)/PS_{68}-*b*-$P4VP_{32}$ system, the shell structure transformed from the coronal spheres to patched spheres (Fig. 5(d)). This was confirmed by staining the micelles

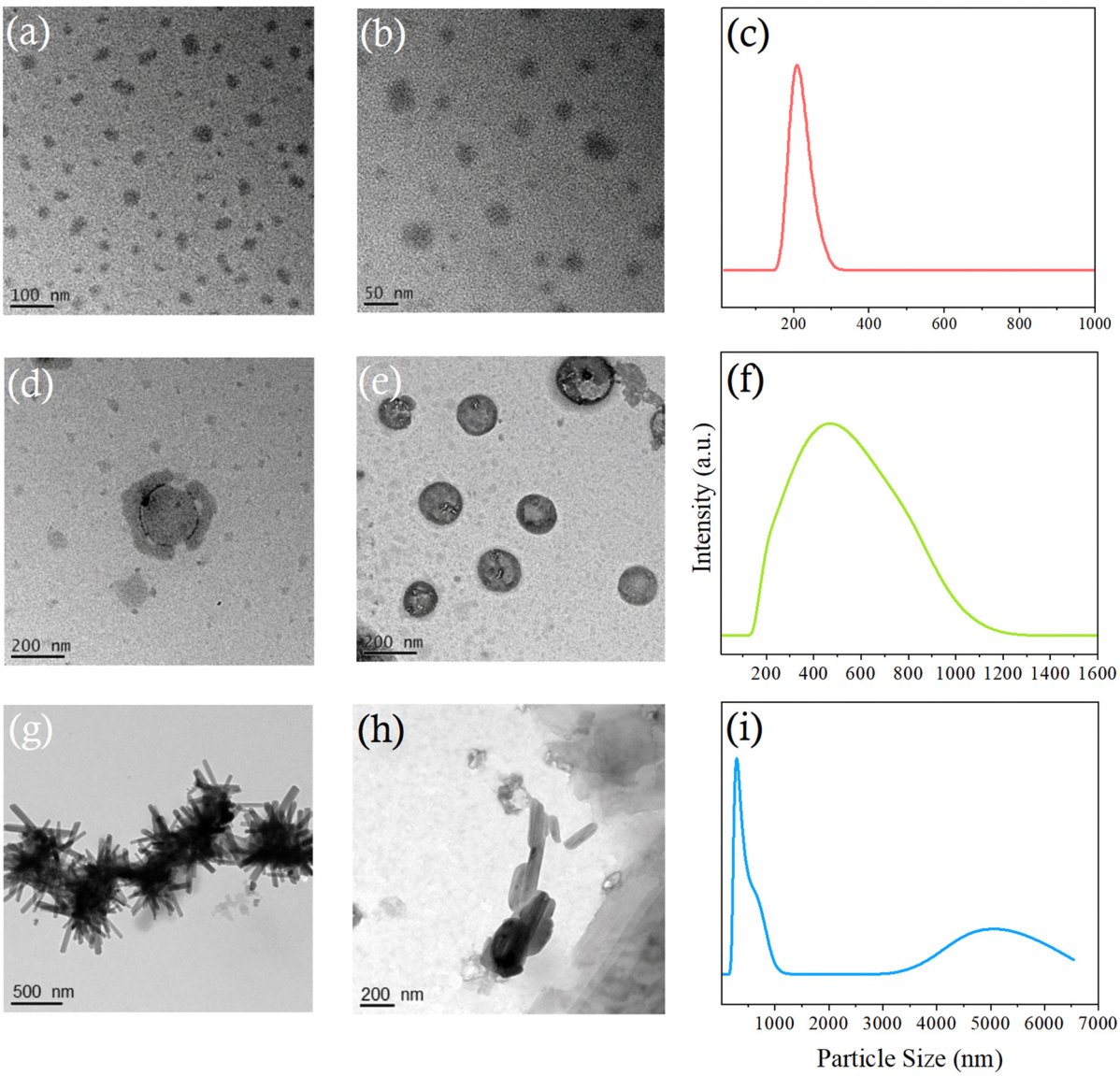

Fig. 5 (a and b) TEM images and (c) DLS analysis results of hydrogen bonding connected micelles, (d and e) TEM images and (f) DLS analysis results of the cross-linked micelles with 1,4-dibromobutane, and (g and h) TEM images and (i) DLS analysis results of the rod-like structures after dissolution in the DMF solution from the poly(S-*alt*-*p*HPMI)/PS_{68}-*b*-$P4VP_{32}$ inter-polymer complex (TEM images in (a, b, d and g) show staining with I_2, and (e and h) show staining with RuO_4).

with I_2, revealing that the P4VP segment was primarily located at the shell region. Furthermore, RuO_4 staining also confirmed the presence of spherical structures, as shown in Fig. 5(e), indicating that the PS segment is located in both the shell and core regions, as illustrated in Scheme 2(h). Finally, we added the same volume of DMF to dissolve the poly(S-*alt*-*p*HPMI) copolymer. Fig. 5(g) and (h) show the appearance of rod-like or worm-like micelles. Additionally, DLS data showed that the poly(S-*alt*-*p*HPMI)/PS_{68}-*b*-$P4VP_{32}$ inter-polymer complexation exhibited a mono-modal distribution both before and after cross-linking (Fig. 5(c) and (f)). However, after cross-linking the poly(S-*alt*-*p*HPMI)/PS_{68}-*b*-$P4VP_{32}$ micelle structures, the particle size increased. This could be attributed to the presence of the free PS block segment expanding the micelle structure. This is different from the pure P4VP homopolymer and PS_{41}-*r*-$P4VP_{59}$ random copolymer systems. Another possible reason for the increase in particle size is the formation of different self-assembled micelle structures, such as rods or worm-like structures, due to the presence of the block copolymer architecture. As a result, a large number of rod-like micelles existed after the removal of the poly(S-*alt*-*p*HPMI) copolymer by the DMF solution, leading to two broader distributions of rod-like micelles detected by DLS. The distribution included a relatively small cross-section length of rod-like micelles at approximately 285 nm and another relatively large hydrodynamic diameter due to the length of rod-like micelles at approximately 5 μm, as shown in Fig. 5(i).[39] Similarly, AFM and FTIR analyses (Fig. S5 and S6, ESI†) exhibit similar morphologies, particle sizes, hydrogen bonding, crosslinking reaction, and the effect of DMF washing on the removal of poly(S-*alt*-*p*HPMI) copolymers for the PS_{68}-*b*-$P4VP_{32}$ system.

Conclusion

We prepared hydrogen bonding connected micelles using a P4VP-deriviate shell and a poly(S-*alt*-*p*HPMI) core in a selective solvent. To adjust the hydrogen bonding interaction sites at the core/shell interface, we synthesized three different sequences of PS-*co*-P4VP copolymers, which mediated hydrogen-bonded acceptors on the shell structures. The TEM images confirmed that self-assembled spherical structures were formed. We used 1,4-dibromobutane as a cross-linking agent to stabilize the PS-*co*-P4VP shell and dissolve the poly(S-*alt*-*p*HPMI) core in DMF to obtain hollow spheres. TEM, DLS, FTIR, and AFM analysis results confirmed the morphologies, particle sizes, hydrogen bonding, crosslinking reaction, and core dissolution. Compared to the poly(S-*alt*-*p*HPMI)/P4VP complex, the poly(S-*alt*-*p*HPMI)/PS_{41}-*r*-$P4VP_{59}$ complex resulted in larger and more irregular hydrogen bonding connected micelles, cross-linked micelles, and hollow spheres due to the random sequences and fewer intermolecular hydrogen bonds at the core/shell interface. Additionally, the poly(S-*alt*-*p*HPMI)/PS_{68}-*b*-$P4VP_{32}$ complex formed rod- or worm-like structures after core dissolution due to the presence of the block copolymer architecture.

Conflicts of interest

There are no conflicts to declare.

Acknowledgements

This study was supported financially by the Ministry of Science and Technology, Taiwan, under contracts NSTC 110-2124-M-002-013 and 111-2223-E-110-004. The authors thank the staff at National Sun Yat-sen University for their assistance with the TEM (ID: EM022600) experiments.

References

1 E. Gravel, J. Ogier, T. Arnauld, N. Mackiewicz, F. Duconge and E. Doris, Drug Delivery and Imaging with Polydiacetylene Micelles, *Chem. – Eur. J.*, 2012, **18**, 400–408, DOI: **10.1002/chem.201102769**.

2 J. Luo, C. Fan, X. Wang, R. Liu and X. Liu, A novel electrochemical sensor for paracetamol based on molecularly imprinted polymeric micelles, *Sens. Actuators, B*, 2013, **188**, 909–916, DOI: **10.1016/j.snb.2013.07.088**.

3 F. Beunis, F. Strubbe, M. Karvar, O. Drobchak, T. Brans and K. Neyts, Inverse micelles as charge carriers in nonpolar liquids: Characterization with current measurements, *Curr. Opin. Colloid Interface Sci.*, 2013, **18**, 129–136, DOI: **10.1016/j.cocis.2013.02.010**.

4 S. Perumal, R. Atchudan and W. Lee, A Review of Polymeric Micelles and Their Applications, *Polymers*, 2022, **14**, 2510, DOI: **10.3390/polym14122510**.

5 A. Mustafai, M. Zubair, A. Hussain and A. Ullah, Recent Progress in Proteins-Based Micelles as Drug Delivery Carriers, *Polymers*, 2023, **15**, 836, DOI: **10.3390/polym15040836**.

6 M. Lu, X. Huang, X. Cai, J. Sun, X. Liu, L. Weng, L. Zhu, Q. Luo and Z. Chen, Hypoxia-Responsive Stereocomplex Polymeric Micelles with Improved Drug Loading Inhibit Breast Cancer Metastasis in an Orthotopic Murine Model, *ACS Appl. Mater. Interfaces*, 2022, **14**, 20551–20565, DOI: **10.1021/acsami.1c23737**.

7 X. Ye, H. Niroomand, S. Hu and B. Khomami, Block copolymer micelle formation in a solvent good for all the blocks, *Colloid Polym. Sci.*, 2015, **293**, 2799–2805, DOI: **10.1007/s00396-015-3658-9**.

8 S. C. Chen, S. W. Kuo and F. C. Chang, On Modulating the Self-Assembly Behaviors of Poly(styrene-*b*-4-vinylpyridine)/Octyl Gallate Blends in Solution State via Hydrogen Bonding from Different Common Solvents, *Langmuir*, 2011, **27**, 10197–10205, DOI: **10.1021/la201506y**.

9 T. C. Chou, W. C. Chen, M. G. Mohamed, Y. C. Huang and S. W. Kuo, Organic-Inorganic Phenolic/POSS Hybrids Provide Highly Ordered Mesoporous Structures Templated by High Thermal Stability of PS-*b*-P4VP Diblock Copolymer, *Chem. – Eur. J.*, 2023, **29**, e202300538, DOI: **10.1002/chem.202300538**.

10 S. W. Kuo, Hydrogen Bonding Mediated Self-Assembled Structures from Block Copolymer Mixtures to Mesoporous Materials, *Polym. Int.*, 2022, **71**, 393–410, DOI: 10.1002/pi.6264.
11 S. W. Kuo, Hydrogen bond-mediated self-assembly and supramolecular structures of diblock copolymer mixtures, *Polym. Inter.*, 2009, **58**, 455–464, DOI: 10.1002/pi.2513.
12 C. J. Hsu, C. W. Tu, Y. W. Huang, S. W. Kuo, R. H. Lee, Y. T. Liu, H. Y. Hsueh, J. Aimi and C. F. Huang, Synthesis of poly (styrene)-*b*-poly (2-vinyl pyridine) four-arm star block copolymers via ATRP and their self-assembly behaviors, *Polymer*, 2021, **213**, 123212, DOI: 10.1016/j.polymer.2020.123212.
13 M. G. Mohamed and S. W. Kuo, Progress in the self-assembly of organic/inorganic polyhedral oligomeric silsesquioxane (POSS) hybrids, *Soft Matter*, 2022, **18**, 5535–5561, DOI: 10.1039/D2SM00635A.
14 S. W. Kuo, Hydrogen bonding interactions in polymer/polyhedral oligomeric silsesquioxane nanomaterials, *J. Polym. Res.*, 2022, **29**, 69, DOI: 10.1007/s10965-021-02885-4.
15 J. F. Gohy, Block Copolymer Micelles, *Adv. Polym. Sci.*, 2005, **190**, 65–136, DOI: 10.1007/12_048.
16 H. Lee and K. Char, Morphological Changes from Silica Tubules to Hollow Spheres Controlled by the Intermolecular Interactions within Block Copolymer Micelle Templates, *ACS Appl. Mater. Interfaces*, 2009, **1**, 913–920, DOI: 10.1021/am900026s.
17 M. Guo and M. Jiang, Non-covalently connected micelles (NCCMs): the origins and development of a new concept, *Soft Matter*, 2009, **5**, 495–500, DOI: 10.1039/B813556H.
18 M. Wang, M. Jiang, F. Ning, D. Chen, S. Liu and H. Duan, Block-Copolymer-Free Strategy for Preparing Micelles and Hollow Spheres: Self-Assembly of Poly(4-vinylpyridine) and Modified Polystyrene, *Macromolecules*, 2002, **35**, 5980–5989, DOI: 10.1021/ma0201330.
19 W. T. Du, E. A. Orabi, M. G. Mohamed and S. W. Kuo, Inter/intramolecular hydrogen bonding mediate miscible blend formation between near-perfect alternating Poly (styrene-*alt*-hydroxyphenylmaleimide) copolymers and Poly(vinyl pyrrolidone), *Polymer*, 2021, **219**, 123542, DOI: 10.1016/j.polymer.2021.123542.
20 W. T. Du, T. L. Ma and S. W. Kuo, Steric hindrance affects interactions of poly(styrene–*alt*–DMHPMI) copolymer with strongly hydrogen-bond-accepting homopolymers, *Polymer*, 2023, **268**, 125694, DOI: 10.1016/j.polymer.2023.125694.
21 W. T. Du and S. W. Kuo, Varying the sequence distribution and hydrogen bonding strength provides highly Heat-Resistant PMMA copolymers, *Eur. Polym. J.*, 2022, **170**, 111165, DOI: 10.1016/j.eurpolymj.2022.111165.
22 T. C. Tseng and S. W. Kuo, Hydrogen-Bonding Strength Influences Hierarchical Self-Assembled Structures in Unusual Miscible/Immiscible Diblock Copolymer Blends, *Macromolecules*, 2018, **51**, 6451–6459, DOI: 10.1021/acs.macromol.8b00751.
23 K. J. Eichhorn, A. Fahmi, G. Adam and M. Stamm, Temperature-dependent FTIR spectroscopic studies of hydrogen bonding of the copolymer poly(styrene-*b*-4-vinylpyridine) with pentadecylphenol, *J. Mol. Struct.*, 2003, **661–662**, 161–170, DOI: 10.1016/S0022-2860(03)00513-1.
24 B. Li, X. Lu, Y. Ma and Z. Chen, Thermo- and pH-responsive behaviors of aqueous poly(acrylic acid)/poly(4-vinylpyridine) complex material characterized by ATR-FTIR and UV–Vis Spectroscopy, *Eur. Polym. J.*, 2014, **60**, 255–261, DOI: 10.1016/j.eurpolymj.2014.09.017.
25 S. W. Kuo, C. L. Lin and F. C. Chang, The study of hydrogen bonding and miscibility in poly (vinylpyridines) with phenolic resin, *Polymer*, 2002, **43**, 3943–3949, DOI: 10.1016/S0032-3861(02)00214-8.
26 S. W. Kuo, P. H. Tung and F. C. Chang, Syntheses and the study of strongly hydrogen-bonded poly (vinylphenol-*b*-vinylpyridine) diblock copolymer through anionic polymerization, *Macromolecules*, 2006, **39**, 9388–9395, DOI: 10.1021/ma061713q.
27 W. C. Chen, S. W. Kuo, C. H. Lu, U. S. Jeng and F. C. Chang, Self-Assembly Structures through Competitive Interactions of Crystalline−Amorphous Diblock Copolymer/Homopolymer Blends: Poly(ε-caprolactone-*b*-4-vinyl pyridine)/Poly(vinyl phenol), *Macromolecules*, 2009, **42**, 3580–3590, DOI: 10.1021/ma900080v.
28 P. Guo, W. Guan, L. Liang and P. Yao, Self-assembly of pH-sensitive random copolymers: Poly(styrene-*co*-4-vinylpyridine), *J. Colloid Interface Sci.*, 2008, **323**, 229–234, DOI: 10.1016/j.jcis.2008.04.009.
29 M. Dan, F. Huo, X. Zhang, X. Wang and W. Zhang, Dispersion RAFT Polymerization of 4-Vinylpyridine in Toluene Mediated with the Macro-RAFT Agent of Polystyrene Dithiobenzoate: Effect of the Macro-RAFT Agent Chain Length and Growth of the Block Copolymer Nano-Objects, *J. Polym. Sci., Part A: Polym. Chem.*, 2013, **51**, 1573–1584, DOI: 10.1002/pola.26527.
30 S. W. Kuo, C. H. Wu and F. C. Chang, Thermal Properties, Interactions, Morphologies, and Conductivity Behavior in Blends of Poly(vinylpyridine)s and Zinc Perchlorate, *Macromolecules*, 2004, **37**, 192–200, DOI: 10.1021/ma035655.
31 D. R. Yei, S. W. Kuo, H. K. Fu and F. C. Chang, Enhanced thermal properties of PS nanocomposites formed from montmorillonite treated with a surfactant/cyclodextrin inclusion complex, *Polymer*, 2005, **46**, 741–750, DOI: 10.1016/j.polymer.2004.11.108.
32 C. F. Huang, S. W. Kuo, J. K. Chen and F. C. Chang, Synthesis and Characterization of Polystyrene-*b*-Poly(4-vinyl pyridine) Block Copolymers by Atom Transfer Radical Polymerization, *J. Polym. Res.*, 2005, **12**, 449–456, DOI: 10.1007/s10965-004-5665-2.
33 L. Tripathi, L. P. Wu, J. Chen and G. Q. Chen, Synthesis of Diblock copolymer poly-3-hydroxybutyrate-*block*-poly-3-hydroxyhexanoate [PHB-*b*-PHHx] by a β-oxidation weakened Pseudomonas putida KT2442, *Microb. Cell Fact.*, 2012, **11**, 44, DOI: 10.1186/1475-2859-11-44.
34 J. M. J. Fréchet and M. V. de Meftahi, Poly(vinyl pyridine)s: Simple reactive polymers with multiple applications, *Br. Polym. J.*, 1984, **16**, 193–198, DOI: 10.1002/pi.4980160407.
35 M. Changez, H. D. Koh, N. G. Kang, J. G. Kim, Y. J. Kim, S. Samal and J. S. Lee, Molecular Level Ordering in Poly(2-vinylpyridine), *Adv. Mater.*, 2012, **24**, 3253–3257, DOI: 10.1002/adma.201201342.
36 C. Nah, K. U. Jeong, Y. S. Lee, S. H. Lee, M. M. A. Kader, H. K. Leed and J. H. Ahne, Polymer electrolyte membranes composed of an electrospun poly(vinylidene fluoride)

fibrous mat in a poly(4-vinylpyridine) matrix, *Polym. Inter.*, 2013, **62**, 375–381, DOI: **10.1002/pi.4311**.

37 G. Zhang, S. Tang, A. Li and L. Zhu, Thermally Stable Metallic Nanoparticles Prepared via Core-Crosslinked Block Copolymer Micellar Nanoreactors, *Langmuir*, 2017, **33**, 6353–6362, DOI: **10.1021/acs.langmuir.7b00573**.

38 S. W. Kuo, *Hydrogen Bonding in Polymeric Materials*, John Wiley & Sons, 2018.

39 S. W. Kuo, P. H. Tung and F. C. Chang, Hydrogen bond mediated supramolecular micellization of diblock copolymer mixture in common solvents, *Eur. Polym. J.*, 2009, **45**, 1924–1935, DOI: **10.1016/j.eurpolymj.2009.03.020**.